Rev. Adv. Mater. Sci. 48 (2017) 156-169

SHEAR BANDING INSTABILITIES IN BULK METALLIC GLASSES AT LOW STRAIN RATES: GRADIENT AND LENGTH SCALE EFFECTS

Ioannis Tsagrakis[1] and Elias C. Aifantis[1-5]

[1]Aristotle University of Thessaloniki, Thessaloniki 54124, Greece
[2]Michigan Technological University, Houghton, MI 49931, USA
[3]Beijing University of Civil Engineering and Architecture, Beijing 100044, China
[4]ITMO University, St. Petersburg 197101, Russia
[5]Togliatti State University, Togliatti 445020, Russia

Received: January 24, 2017

Abstract. Shear banding in metallic glasses under low strain rates is discussed by elaborating on the coupling of the underlying thermal and free volume diffusion with plastic strain gradients. Linear stability analysis is employed to examine the interplay between strain, temperature and free volume internal lengths on the onset of instability, as this is determined within a multiphysics / multiscale system of partial differential equations of the reaction – diffusion (R-D) type. Size-dependent stability criteria are derived and size-dependent diagrams are constructed indicating that shear banding can be completely suppressed below a critical (nanoscale) size in accordance with experimental trends found in the literature. These results are qualitatively similar to those observed in nanocrystalline and ultrafine grain polycrystals.

The effect of the different length scales on the shear band thickness is also investigated by solving the system of governing equations numerically using the method of lines along with the spectral element method. It is found that free volume diffusion controls the development of nanoscale shear bands, while strain gradients govern the evolution and morphology of micron-scale shear bands that have been reported in the literature. In both cases the influence of thermal diffusion turns out to be negligible for the quasi-static loading conditions considered herein. This is in contrast to most of the previous adiabatic shear banding stability analyses of various authors which resorted to thermal diffusion and heat conductivity to deduce stability criteria for thermally softening materials.

1. INTRODUCTION

Bulk metallic glasses (BMGs) constitute an emerging class of materials with excellent mechanical properties such as high strength/hardness and corrosion resistance. However, below the glass-transition temperature and at high stresses, plastic deformation is localized into microscale and/or nanoscale shear bands, which in turn act as precursors to crack formation, rendering limited ductility before catastrophic failure [1]. The complex spatio-temporal inhomogeneous nature of shear banding in BMGs leads to irregular (jerky) plastic flow and corresponding serrated stress-strain curves, commonly observed at low strain/loading rates in compression and indentation tests [2]. This type of plastic deformation is characterized by a “slow” elastic loading part followed by “fast” stress drops which reflect the occurrence of an intermittent instability event, such as stick-slip propagation of a single dominant shear band [1] or activation of multiple individual shear bands [3].

The most widely used phenomenological models of deformation in metallic glasses are based ei-

Corresponding author: Elias C. Aifantis, e-mail: mom@mom.gen.auth.gr

ther on the concept and mechanism of free volume/FV [4-6], or on the concept and mechanism of shear transformation zone/STZ [7] and its extensions (e.g. the two-state STZ model [8] and cooperative shear model [9]). Other models are also available such as those based on an effective disorder temperature [10], as well as those based on atomistic and molecular dynamics [11,12]. Despite the differences in the material parameters employed and their emphasis on different aspects of the glass state and associated structural processes, most of these models have the common feature of using an *internal variable* (i.e. free volume, configurational potential energy density, or effective disorder temperature) characterizing the material substructure. Accordingly, complex microstructural changes caused by plastic deformation are taken into account by postulating appropriate evolution laws (with or without diffusive transport) for the corresponding internal variables. These in combination with the balance equations for momentum and energy, lead to a set of coupled differential equations governing the material loading response.

In such a framework, temperature gradients arise naturally for inhomogeneous deformation through the energy balance (heat conduction) equation and free volume microstructural spatial gradients though a diffusive-like term in the evolution equation for the internal variable (FV and/or STZ) [13,14]. In this connection, it is noted that diffusive-like evolution equations for internal variables (including vacancies, free volume, pores and voids) were proposed by Aifantis over thirty five years ago [15] in order to capture heterogeneity of plastic flow and damage within a generalized continuum mechanics framework (see also [16] and references quoted therein). However, no application of such an approach to metallic glasses was utilized until the works of Huang et al. [17], Dai et al. [18], and Jiang et al. [14] where a diffusion term was introduced into the evolution equation for the free volume. This term provides an internal length scale parameter and a corresponding gradient that stabilizes the material behavior in the softening regime, and hence the model becomes able to predict shear band spacings and shear offsets [13], in analogy to the predictions of shear band widths and spacings provided by the strain gradient plasticity model of Aifantis [19,20] for metals.

In fact, the present article elaborates on a "missing link" between the aforementioned gradient theories for metallic glasses and the strain gradient theory of metal plasticity. This is done by considering the effect of free volume, temperature, and strain gradients – strictly speaking, the interplay of the Laplacians of these three constitutive variables – on equal footing when constructing the system of the governing equations for the deformed material state under slow strain rates, temperature and free volume changes. In this way, shortcomings of classical plastic flow models such as the indetermination of shear band width/spacings, the ill-posedness of corresponding boundary value problems and the associated spurious discretization sensitivity when the material enters the softening regime are removed due to the introduction of the Laplacians, in analogy to the case of metal plasticity [21,22].

It is due to the above advantages that strain gradient plasticity of the "Laplacian-type" has been extensively used in strain localization analyses of various classes of materials, ranging from single crystal and polycrystalline metals to polymers and geological materials. However, there are no related studies in the literature of metallic glasses and the present work – along with a companion forthcoming one [23] – can be considered as an initial attempt to deal with this lack by coupling gradient viscoplasticity, heat conduction and free volume diffusion for simple shearing deformations at low strain rates. The interplay between strain, temperature and free volume internal lengths on the onset of instability is examined by employing linear stability analysis, in accordance with a standard procedure in shear banding literature (e.g. [24,25] and references quoted therein, for polycrystalline metals, as well as in [17,18,26] for metallic glasses). Then, attention is focused on size effects and size-dependent stability diagrams are derived. Furthermore, the contribution of the three intrinsic lengths scales on the shear band thickness is discussed by solving the system of governing equations numerically in the post-localization regime. It is emphasized that the analysis presented is applicable to other types of thermo-visco-plastic gradient materials where the internal variable (FV) used for bulk metallic glasses is replaced by another pertinent internal variable with diffusive transport; e.g. void density in the case of degradation or healing of materials with damage.

2. GOVERNING EQUATIONS

We consider the simple shearing deformation of an isotropic and homogeneous bulk metallic glass occupying the region $0 \le y \le L$, $x, z \in \mathbb{R}$ and sheared in the x-direction. The strain rate applied is assumed low enough, so that inertia effects can be neglected. The model equations describing the evolution of stress/strain, temperature and free volume density (internal variable) are

$$\frac{\partial \tau}{\partial y} = 0;$$
$$\rho c_v \frac{\partial \theta}{\partial t} = k \frac{\partial^2 \theta}{\partial y^2} + F(\xi, \theta, \tau);$$
$$\frac{\partial \xi}{\partial t} = D \frac{\partial^2 \xi}{\partial y^2} + G(\xi, \theta, \tau). \qquad (1)$$

$$\tau = \kappa(\gamma^p, \dot{\gamma}^p, \theta, \xi) - c \frac{\partial^2 \gamma^p}{\partial y^2};$$
$$\gamma = \frac{\tau}{\mu} + \gamma^p. \qquad (2)$$

$$\frac{\partial \tilde{\tau}}{\partial y} = 0;$$
$$\frac{\partial \tilde{\theta}}{\partial \tilde{t}} = \ell_\theta^2 \frac{\partial^2 \tilde{\theta}}{\partial y^2} + \tilde{\beta} \tilde{\tau} \tilde{\dot{\gamma}}^p;$$
$$\frac{\partial \xi}{\partial \tilde{t}} = \ell_\xi^2 \frac{\partial^2 \xi}{\partial y^2} + \tilde{G}(\xi, \tilde{\theta}, \tilde{\tau}), \qquad (3)$$

$$\tilde{\tau} = \tilde{\kappa}(\gamma^p, \tilde{\dot{\gamma}}^p, \tilde{\theta}, \xi) - \ell_\gamma^2 \frac{\partial^2 \gamma^p}{\partial y^2};$$
$$\gamma = \frac{\tilde{\tau}}{\tilde{\mu}} + \gamma^p, \qquad (4)$$

The first three are the balance equations for the momentum (equilibrium, under quasi-static conditions), the energy, and the free volume, respectively. The fourth is a gradient-dependent constitutive equation for the flow stress [20,27], with *c* being a force-like coefficient. The fifth equation is the standard linear decomposition of the total strain in its elastic and plastic components. Thus, $(\gamma, \dot{\gamma})$ denote the total strain and its rate, while $(\gamma^p, \dot{\gamma}^p)$ denote their plastic counterparts, and τ/μ is the elastic strain with μ being the elastic shear modulus. The internal variable ξ that obeys the reaction-diffusion equation [i.e., Eq.$(1)_3$] is a dimensionless measure of the free volume density. In particular, $\xi = \upsilon_f/\alpha\upsilon^*$, where υ^* is a critical volume (hard-sphere volume of an atom), υ_f is the average free volume per atom, and α is a geometrical factor of order 1. The parameters (ρ, c_v, k, D) denote respectively the mass density, the specific heat, the thermal conductivity, and the free volume diffusion coefficient. The source terms $F(\xi,\theta,\tau)$ and $G(\xi,\theta,\tau)$ represent the net generation rates of heat and free volume, respectively. Usually, the heat source term has the form $F(\xi,\theta,\tau) = \beta\tau\dot{\gamma}^p$, where β is the Taylor-Quinney coefficient that represents the fraction of the rate of plastic work transformed into heat. Explicit expressions for $G(\xi,\theta,\tau)$ are available in the literature, as those proposed by Spaepen [4] and Johnson et al. [6]. It is also noted that the heat conduction equation, i.e. Eq. $(1)_2$, involves a certain number of assumptions, which have been described in detail in [25] and can be considered valid for the slow strain rates discussed here.

Let t_o, θ_o, τ_o denote reference values of time, temperature and stress, respectively. These are introduced to normalize the governing equations, and their explicit expressions depend on the material parameters included in the constitutive equations for the flow stress $\kappa(\gamma^p, \dot{\gamma}^p, \theta, \xi)$ and the free volume generation $G(\xi,\theta,\tau)$. Then, Eqs.(1) and (2) are written in a normalized form as

where the dimensionless variables are defined as follows: shear stress $\tilde{\tau} = \tau/\tau_o$; temperature $\tilde{\theta} = \theta/\theta_o$; time $\tilde{t} = t/t_o$; plastic shear strain rate $\tilde{\dot{\gamma}}^p = \dot{\gamma}^p t_o$, while $\tilde{\beta} = \beta\tau_o/\rho c_v \theta_o$; $\tilde{\mu} = \mu/\tau_o$; $\tilde{G} = G t_o$; $\tilde{\kappa} = \kappa/\tau_o$. It is noted that the space variable *y* remains not normalized, while the parameters $\ell_\theta = \sqrt{k t_o / \rho c_v}$, $\ell_\xi = \sqrt{D t_o}$ and $\ell_\gamma = \sqrt{c/\tau_o}$ define intrinsic length scales which are associated with the presence of the three different second-order spatial derivative terms (heat conduction, free volume diffusion, and strain gradient viscoplasticity).

Moreover, for later use, let us define the following normalized quantities: plastic strain modulus/hardening parameter $\tilde{h} = \partial\tilde{\kappa}/\partial\gamma^p \geq 0$, plastic strain rate sensitivity/hardening parameter $\tilde{s} = \partial\tilde{\kappa}/\partial\tilde{\dot{\gamma}}^p > 0$ thermal softening parameter $\tilde{\Phi} = -\partial\tilde{\kappa}/\partial\tilde{\theta} > 0$, and free volume softening parameter $\tilde{\Xi} = -\partial\tilde{\kappa}/\partial\xi > 0$. Since $\tilde{G}(\xi, \tilde{\theta}, \tilde{\tau})$ is a function of $\xi, \tilde{\theta}$ and $\tilde{\tau}$, we can also define the following parameters: $\tilde{G}_\xi = \partial\tilde{G}/\partial\xi$, $\tilde{G}_{\tilde{\theta}} = \partial\tilde{G}/\partial\tilde{\theta}$, and $\tilde{G}_{\tilde{\tau}} = \partial\tilde{G}/\partial\tilde{\tau}$. It is noted that by assuming $\tilde{h} \geq 0$ and $\tilde{s} > 0$, material instabilities associated directly to local strain softening (Lüders bands) or strain rate softening (Portevin-Le Chatelier bands) are excluded from the present analysis, i.e. only thermal and microstructural free volume softening are considered.

3. LINEAR STABILITY ANALYSIS

Linear stability analysis has been a standard tool in addressing the emergence of pattern formation in chemical and fluid systems. Subsequently, the method has been used to address a variety of thermo-mechanical and chemo-mechanical instabilities in solids [20,21,24,25,27-32] including studies on metallic glasses [17,18,26]. Adopting such a linear stability approach, we look for solutions of Eqs.(3) and (4) in the form

$$\left[\gamma,\gamma^p,\tilde{\theta},\xi,\tilde{\tau}\right]=\left[\gamma_h,\gamma_h^p,\tilde{\theta}_h,\xi_h,\tilde{\tau}_h\right]+ \varepsilon\left[\delta\gamma,\delta\gamma^p,\delta\tilde{\theta},\delta\xi,\delta\tilde{\tau}\right], \quad (5)$$

where the subscript *h* denotes the corresponding time-dependent homogeneous solution, ε is a small parameter and the perturbations $\delta\gamma$, $\delta\gamma^p$, $\delta\tilde{\theta}$, $\delta\xi$ and $\delta\tilde{\tau}$ are functions of both *y* and $\tilde{t}$. Substitution of Eq. (5) into Eqs. (4) and linearization around the homogeneous solution (obtained at the normalized time $\tilde{t}_h$ of the initiation of the perturbation) give $\delta\tilde{\tau}$ and $\delta\gamma$ in terms of $\delta\gamma^p$, $\delta\tilde{\theta}$ and $\delta\xi$ as

$$\delta\tilde{\tau}=\tilde{h}\delta\gamma^p+\tilde{s}\frac{\partial\delta\gamma^p}{\partial\tilde{t}}-\tilde{\Phi}\delta\tilde{\theta}- \tilde{\Xi}\delta\xi-\ell_\gamma^2\frac{\partial^2\delta\gamma^p}{\partial y^2}; \quad \delta\gamma=\frac{\delta\tilde{\tau}}{\tilde{\mu}}+\delta\gamma^p, \quad (6)$$

Accordingly, the system of the first-order approximation deduced from Eqs.(3) can be written only with respect $\delta\gamma^p$, $\delta\tilde{\theta}$ and $\delta\xi$ as

$$\tilde{h}\frac{\partial\delta\gamma^p}{\partial y}+\tilde{s}\frac{\partial^2\delta\gamma^p}{\partial y\partial\tilde{t}}-\tilde{\Phi}\frac{\partial\delta\tilde{\theta}}{\partial y}-\tilde{\Xi}\frac{\partial\delta\xi}{\partial y} -\ell_\gamma^2\frac{\partial^3\delta\gamma^p}{\partial y^3}=0, \quad (7)$$

$$\frac{\partial\delta\tilde{\theta}}{\partial\tilde{t}}=\ell_\theta^2\frac{\partial^2\delta\tilde{\theta}}{\partial y^2}+\tilde{\beta}\left[(\tilde{\tau}_h+\tilde{s}\tilde{\gamma}_h^p)\frac{\partial\delta\gamma^p}{\partial\tilde{t}}+\tilde{h}\tilde{\gamma}_h^p\delta\gamma^p- \tilde{\Phi}\tilde{\gamma}_h^p\delta\tilde{\theta}-\tilde{\Xi}\tilde{\gamma}_h^p\delta\xi-\ell_\gamma^2\tilde{\gamma}_h^p\frac{\partial^2\delta\gamma^p}{\partial y^2}\right], \quad (8)$$

$$\frac{\partial\delta\xi}{\partial\tilde{t}}=\ell_\xi^2\frac{\partial^2\delta\xi}{\partial y^2}+\left(\tilde{G}_\xi-\tilde{G}_{\tilde{\tau}}\tilde{\Xi}\right)\delta\xi+\left(\tilde{G}_{\tilde{\theta}}-\tilde{G}_{\tilde{\tau}}\tilde{\Phi}\right)\delta\tilde{\theta} +\tilde{G}_{\tilde{\tau}}\left(\tilde{h}\delta\gamma^p+\tilde{s}\frac{\partial\delta\gamma^p}{\partial\tilde{t}}-\ell_\gamma^2\frac{\partial^2\delta\gamma^p}{\partial y^2}\right). \quad (9)$$

This system is linear with constant coefficients with respect to *y*. Therefore, for an infinite domain (i.e., $y\in\mathbb{R}$) and assuming that perturbations remain bounded as $y\to\pm\infty$, we can apply the Fourier transform from the spatial domain of *y* to the wavenumber domain of *q*. This is equivalent with the use of the ansatz

$$\delta\gamma^p(y,\tilde{t})=\overline{\gamma}^p(\tilde{t})e^{iqy},\quad \delta\tilde{\theta}(y,\tilde{t})=\overline{\theta}(\tilde{t})e^{iqy},\quad \delta\xi(y,\tilde{t})=\overline{\xi}(\tilde{t})e^{iqy}. \quad (10)$$

Substitution of Eqs. (10) into Eqs. (7)-(9) gives

$$\frac{d\overline{\gamma}^p}{d\tilde{t}}=-\left(\frac{\tilde{h}+\ell_\gamma^2q^2}{\tilde{s}}\right)\overline{\gamma}^p+\frac{\tilde{\Phi}}{\tilde{s}}\overline{\theta}+\frac{\tilde{\Xi}}{\tilde{s}}\overline{\xi}, \quad (11)$$

$$\frac{d\overline{\theta}}{d\tilde{t}}=-\tilde{\beta}\tilde{\tau}_h\frac{\tilde{h}+\ell_\gamma^2q^2}{\tilde{s}}\overline{\gamma}^p+\left(\tilde{\beta}\tilde{\tau}_h\frac{\tilde{\Phi}}{\tilde{s}}-\ell_\theta^2q^2\right)\overline{\theta}+ \tilde{\beta}\tilde{\tau}_h\frac{\tilde{\Xi}}{\tilde{s}}\overline{\xi}, \quad (12)$$

$$\frac{d\overline{\xi}}{d\tilde{t}}=\left(\tilde{G}_\xi-\ell_\xi^2q^2\right)\overline{\xi}+\tilde{G}_{\tilde{\theta}}\overline{\theta}. \quad (13)$$

This is a homogeneous linear system of first-order differential equations which can be written in the form $\dot{\mathbf{s}}(\tilde{t})=\mathbf{A}(\tilde{t}_h,q)\mathbf{s}(\tilde{t})$, where $\mathbf{s}(\tilde{t})=\left[\overline{\gamma}^p(\tilde{t}),\overline{\theta}(\tilde{t}),\overline{\xi}(\tilde{t})\right]^T$, while the matrix $\mathbf{A}(\tilde{t}_h,q)$ depends on the homogeneous solution at the time $\tilde{t}_h$ of the initiation of the perturbation and thus, on γ_h through the coefficients $\tilde{h},\tilde{s},\tilde{\Phi},\tilde{\Xi},\tilde{\tau}_h,\tilde{G}_\xi$ and $\tilde{G}_{\tilde{\theta}}$. Accordingly, this system admits solutions of the form

$$\mathbf{s}(\tilde{t})=\left[\hat{\gamma}^p(\tilde{t}_h,q),\hat{\theta}(\tilde{t}_h,q),\hat{\xi}(\tilde{t}_h,q)\right]^T e^{\omega(\tilde{t}_h,q)(\tilde{t}-\tilde{t}_h)}, \quad (14)$$

where $\omega=\omega(\tilde{t}_h,q)$ is the normalized perturbation growth rate at time $\tilde{t}_h$. Substituting $\mathbf{s}(\tilde{t})$ into Eqs. (11)-(13), we obtain a set of linear equations of the form **MX**=**0**, with

$$\mathbf{M}=\begin{bmatrix}\tilde{s}\omega+\tilde{h}+\ell_\gamma^2q^2 & -\tilde{\Phi} & -\tilde{\Xi}\\ \tilde{\beta}\tilde{\tau}_h\omega & -(\omega+\ell_\theta^2q^2) & 0\\ 0 & \tilde{G}_{\tilde{\theta}} & \tilde{G}_\xi-\omega-\ell_\xi^2q^2\end{bmatrix}, \quad (15)$$

and $\mathbf{X}=\left[\hat{\gamma}^p,\hat{\theta},\hat{\xi}\right]^T$. This system has non-trivial solution if and only if the determinant of the matrix coefficient **M** is equal to zero. This leads to the following characteristic (spectral) equation

$$\omega^3+a_2\omega^2+a_1\omega+a_0=0, \quad (16)$$

with the various coefficients of the cubic polynomial given by the expressions

$$a_2 = \frac{q^2\left[\ell_\gamma^2 + \tilde{s}(\ell_\theta^2 + \ell_\xi^2)\right] + \tilde{h} - \tilde{\beta}\tilde{\Phi}\tilde{\tau}_h - \tilde{s}\tilde{G}_\xi}{\tilde{s}},$$
$$a_1 = \frac{\left(q^2\ell_\xi^2 - \tilde{G}_\xi\right)\left[q^2(\ell_\gamma^2 + \tilde{s}\ell_\theta^2) + \tilde{h} - \tilde{\beta}\tilde{\Phi}\tilde{\tau}_h\right] + q^2\ell_\theta^2(\tilde{h} + q^2\ell_\gamma^2) - \tilde{\beta}\tilde{\Xi}\tilde{G}_{\tilde{\theta}}\tilde{\tau}_h}{\tilde{s}}, \quad (17)$$
$$a_0 = \frac{q^2\ell_\theta^2(\tilde{h} + q^2\ell_\gamma^2)(q^2\ell_\xi^2 - \tilde{G}_\xi)}{\tilde{s}}.$$

An obvious assumption adopted in the analysis above, as well as in numerous other works on shear banding [25,28,32], including metallic glasses [18], is that the homogeneous solution varies slowly with time as compared to the perturbations, i.e. the homogeneous solution remains "frozen" in $\tilde{t}_h$ and, thus, Eqs. (11)-(13) can be written in the form $\dot{\mathbf{s}}(\tilde{t})=\mathbf{A}(\tilde{t}_h)\mathbf{s}(\tilde{t})$, instead of $\dot{\mathbf{s}}(\tilde{t})=\mathbf{A}(\tilde{t})\mathbf{s}(\tilde{t})$. In fact, this assumption is crucial because otherwise we would have to deal with a linear but non-autonomous system for which the eigenvalues $\omega(\tilde{t})$ of $\mathbf{A}(\tilde{t})$ cannot be used as a measure of stability. As discussed in [25], alternative (but not so straightforward) tools of stability analysis can be utilized. Nevertheless, the assumption of a "frozen" homogeneous solution seems plausible for the low strain rates considered herein. In this case, the question of stability of the initial linearized system of differential equations becomes basically an algebraic problem, as it reduces to the investigation of the sign of the real part of the roots of the cubic polynomial in Eq. (16). Using the Routh-Hurwitz criterion, it is deduced that all the roots of this polynomial equation have negative real parts (indicating stable homogeneous deformation) if and only if all of the following conditions hold true

$$a_2 > 0,$$
$$a_0 > 0, \quad (18)$$
$$a_2 a_1 - a_0 > 0.$$

These, in turn, lead to the inequalities:

$$q^2 > \frac{\tilde{\beta}\tilde{\Phi}\tilde{\tau}_h + \tilde{s}\tilde{G}_\xi - \tilde{h}}{\left[\ell_\gamma^2 + \tilde{s}(\ell_\theta^2 + \ell_\xi^2)\right]},$$
$$q^2 > \frac{\tilde{G}_\xi}{\ell_\xi^2}, \quad (19)$$
$$b_3 q^6 + b_2 q^4 + b_1 q^2 + b_0 > 0.$$

where $b_3 = (\ell_\gamma^2 + \tilde{s}\ell_\theta^2)(\ell_\theta^2 + \ell_\xi^2)(\ell_\gamma^2 + \tilde{s}\ell_\xi^2) > 0$, while the coefficients (b_2,b_1,b_0) are not given here due to their lengthy form.

The violation of the second condition in Eqs. (19) corresponds to a Turing instability (a real eigenvalue crosses zero at marginal stability, i.e. $\omega_c=0$ with $q_c\neq 0$). In the present case we have $q_c = \sqrt{\tilde{G}_\xi}\,/\,\ell_\xi$ and the corresponding symmetry-breaking instability has the characteristic length $l_c = 2\pi / q_c = 2\pi\ell_\xi / \sqrt{\tilde{G}_\xi}$. Moreover, in the original (dimensional) terms Eq. $(19)_2$ is equivalent to $t_D<t_G$, where $t_D=1/Dq^2$ is a characteristic time for the free volume perturbation diffusion, and $t_G=1/G_\xi$ is the characteristic time for the free volume coalescence. Accordingly, Eq. $(19)_2$ expresses the competition between these two processes. When this condition is violated (i.e. $t_D>t_G$), the coalescence process is faster than diffusion and the perturbation will grow leading to the instability of the uniform deformation. In this connection, it is noted that the same instability criterion also appears when isothermal conditions are considered. As discussed in [18], the same holds also when the strain gradient term is not included in the flow stress and the inertia effects are not negligible.

The violation of the third condition in Eqs. (19) corresponds, in general, to a pair of complex conjugate eigenvalues crosses the imaginary axis at criticality, i.e. $\mathrm{Re}(\omega_c)=0$, $\mathrm{Im}(\omega_c)=\sqrt{a_1}\neq 0$ corresponding to another critical wavenumber $q_c\neq 0$. This suggests the emergence of a time symmetry-breaking instability representing a Hopf bifurcation.

As it may be deduced from Eqs.(19), there is a maximum wave number q_{max}, such that the homogeneous solution is stable $\forall\, q > q_{max}$. This, in turn, implies the appearance of a size effect. In particular, for finite domains (e.g. for a layer of thickness L), the boundary conditions will constrain the set of allowable wave numbers q . Considering, for example, that adiabatic conditions and no diffusion flux of the free volume prevail on the boundary along with zero plastic strain gradients, the admissible perturbations will be as in Eq. (10) but with the exponential term e^{iqy} being replaced by $\cos(n\pi y/L)$, $n \in \mathbb{R}$. Then, it can be easily shown that the dispersion relation given by Eqs. (16) and (17) still holds, but with $q=n\pi/L$. Accordingly, the aforementioned condition $q>q_{max}$ implies $L< n\pi/q_{max}$, $\forall n \in \mathbb{N}$, i.e. the homogeneous deformation remains stable to any perturbation when the specimen size is smaller than $L_{min} := \pi/q_{max}$.

4. STABILITY DIAGRAMS AND SIZE EFFECTS

For further illustrating the results of linear stability analysis, substantiating the aforementioned remarks and discuss the occurrence of size effects, we adopt the following explicit expressions for the free volume generation term G and the flow stress κ

$$G(\xi,\theta,\tau) = \frac{1}{\alpha} f \exp\left(-\frac{\Delta G^m}{k_B\theta} - \frac{1}{\xi}\right) \left\{\frac{2k_B\theta}{\upsilon^* S\xi}\left[\cosh\left(\frac{\tau\Omega}{2k_B\theta}\right)-1\right]-\frac{1}{n_D}\right\}, \tag{20}$$

$$\kappa(\dot{\gamma}^p,\theta,\xi) = \frac{2k_B\theta}{\Omega}\operatorname{arcsinh}\left[\frac{\dot{\gamma}^p}{2f}\exp\left(\frac{\Delta G^m}{k_B\theta}+\frac{1}{\xi}\right)\right]. \tag{21}$$

These expressions were introduced by Spaepen [4] based on microscopic arguments for the free volume theory of metallic glasses. The material parameters appearing in Eqs. (20) and (21) are defined as follows: f is the frequency of atomic vibration (~Debye frequency), and ΔG^m is the activation energy of an atom jump; k_B is the Boltzmann constant, and $S=2\mu(1+\nu)/3(1-\nu)$ with μ denoting as before shear modulus and ν being the Poisson's ratio; Ω is the atomic volume and n_D is the number of atomic jumps necessary to annihilate a free volume equal to υ^* usually taken to be 3-10 [26]. It is noted that the homogeneous part of the flow stress given by Eq.(21) does not depend explicitly on the plastic strain γ^p, since a typical BMG stress–strain curve in compression usually consists of an elastic part followed by yielding and perfect plasticity, i.e. $\tilde{h}=0$. The absence of plastic strain hardening can be rationalized by the absence of dislocations in an amorphous material. However, there have been some experiments suggesting this may not be always the case (e.g. [33] and references quoted therein).

Suitable values of the material constants are obtained from the literature (e.g. [14] and references quoted therein) and they are given in Table 1 for a typical $Zr_{41.2}Ti_{13.8}Cu_{12.5}Ni_{10}Be_{22.5}$ bulk metallic glass (Vitreloy 1). Moreover, in what follows, the value c=5 N is used for the calculations, unless otherwise stated.

Following [5] (see also [14], [26]), the reference values t_o, θ_o, τ_o that have been used to normalize the governing equations in the above sections are defined as follows: $t_o = f^{-1}\exp(\Delta G^m/k_B\theta_o) \sim 10^{-5}$ sec, $\tau_o = 2k_B\theta_o/\Omega \sim 414$ MPa with θ_o=300K being the initial temperature.

Eqs. (3) and (4) imply that the homogeneous deformation $\{\gamma_h(\tilde{t}), \gamma_h^p(\tilde{t}), \tilde{\theta}_h(\tilde{t}), \xi_h(\tilde{t}), \tilde{\tau}_h(\tilde{t})\}$ is the solution of the following system of coupled ODEs

$$\begin{aligned} \frac{d\gamma_h}{d\tilde{t}} &= \tilde{\dot{\gamma}}_0 = const., \\ \frac{d\gamma_h^p}{d\tilde{t}} &= \tilde{\psi}(\xi_h, \tilde{\theta}_h, \tilde{\tau}_h), \\ \frac{d\tilde{\theta}_h}{d\tilde{t}} &= \tilde{\beta}\tilde{\tau}_h\tilde{\psi}(\xi_h, \tilde{\theta}_h, \tilde{\tau}_h), \end{aligned} \tag{22}$$

Table 1. Values of Material Constants Used.

ρ	c_v	k	β	D	μ	ν	f
6125	400	20	0.9	10^{-16}	35.3	0.36	~10^{13}
Kg/m^3	J/(kg K)	W/(m K)		m^2/s	GPa		s^{-1}

ΔG^m	Ω	υ^*	n_D	α
0.2-0.5	20	14.12	3	0.15
eV	Å^3	Å^3		

$$\frac{d\xi_h}{d\tilde{t}} = \tilde{G}(\xi_h, \tilde{\theta}_h, \tilde{\tau}_h),$$
$$\frac{d\tilde{\tau}_h}{d\tilde{t}} = \tilde{\mu}[\dot{\tilde{\gamma}}_o - \tilde{\psi}(\xi_h, \tilde{\theta}_h, \tilde{\tau}_h)], \quad (23)$$

where $\tilde{\dot{\gamma}}_o = \dot{\gamma}_o t_o$ with $\dot{\gamma}_o$ the applied strain rate, and $\tilde{\dot{\gamma}}_h^p = \tilde{\psi}(\xi_h, \tilde{\theta}_h, \tilde{\tau}_h)$ is the solution of $\tilde{\tau}_h = \tilde{\kappa}(\tilde{\dot{\gamma}}_h^p, \tilde{\theta}, \xi)$ with respect to $\tilde{\dot{\gamma}}_h^p$. Then, the system can be numerically integrated to find the homogeneous solution. The obtained results for $\tilde{\tau}_h, \xi_h, \tilde{\theta}_h$ and γ_h^p vs. the total strain γ_h are depicted in Fig. 1, using the shear strain rate $\dot{\gamma}_o = 10^{-2}$ s^{-1}. Similar results can be found, for example, in [14] and [26], along with a thorough discussion on the various effects contributing to their form.

Next, the numerical results for the homogeneous solution are used to check the stability conditions, i.e. Eqs.(19), in the course of deformation. These provide the stability diagrams of shear strain (γ_h) vs. wave number (q), as depicted in Fig. 2, where different values of the free volume diffusion coefficient D are used, i.e. 100, 200 and 300 nm^2/s corresponding to ℓ_ξ =0.0315, 0.0445 and 0.0545 nm, respectively. As shown, there is a strong influence of D on the instability regime, which is due to the fact that the major part of this regime comes from the violation of Eq. $(19)_2$. Only for wave numbers less than ~50 m^{-1} the violation of Eq. $(19)_3$ is a necessary and sufficient condition of instability. Testing various values of the thermal conductivity k in the range 0-1000 W/(mK) reveals that this wave number is highly reduced as k increases, while its value for k=0 is ~$4\cdot10^4$ m^{-1}. However, the corresponding effect on the instability initiation is minor, i.e. the violation of Eq. $(19)_3$ begins at $\gamma_h \cong 0.0184$ while the violation of Eq. $(19)_2$ in the same wave number interval at $\gamma_h \cong 0.019$. Similarly, testing various values of the strain gradient coefficient c in the range 0-1000 N shows a non-considerable effect on the instability regime.

As mentioned above, for finite domains of thickness L, the wave numbers can take only discrete values of the form $q = n\pi/L$. Substituting this relation in Eqs. (19) and demanding the resulting inequalities to hold $\forall n \in \mathbb{N}$, leads to the stability diagram of Fig. 3.

It follows that smaller specimens can support larger stable homogeneous deformations even in the softening regime (i.e. for γ_h>0.04). This effect becomes more pronounced as the value of D increases,

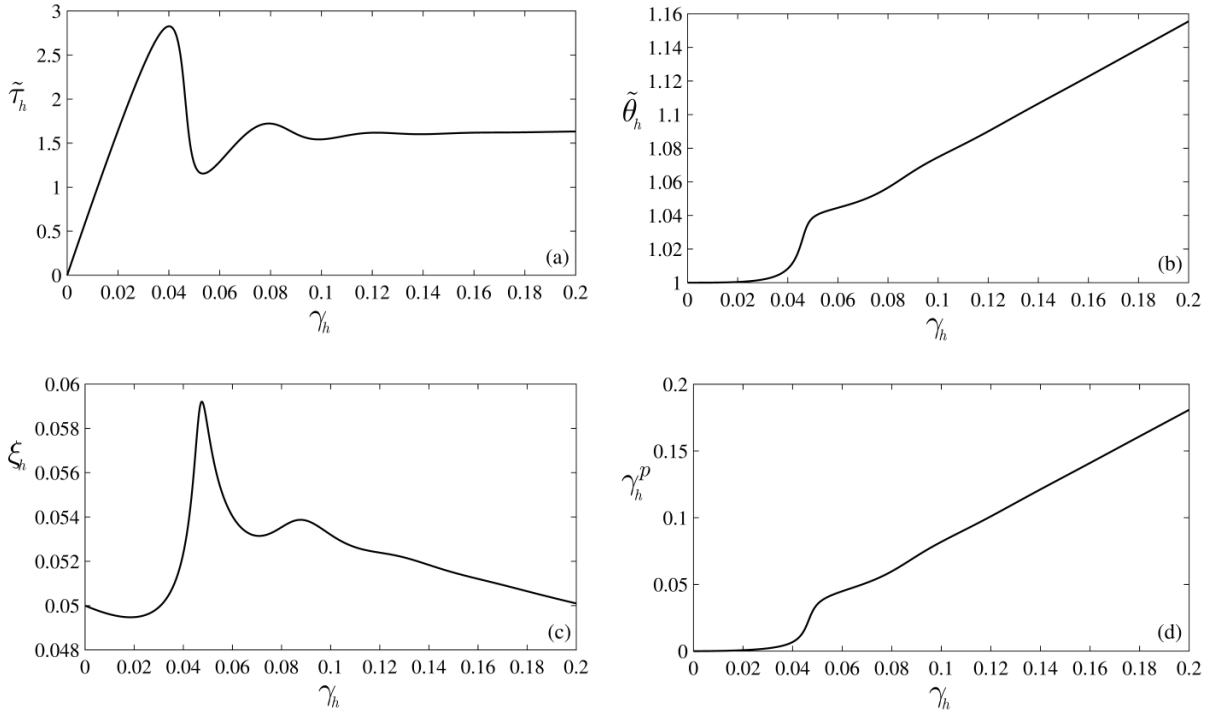

Fig. 1. Homogeneous solution at $\dot{\gamma}_o = 10^{-2}$ s^{-1}: Normalized stress, temperature, free volume and plastic strain versus the applied shear strain. It is noted that a maximum (outburst) occurs for the stress and free volume, while temperature and plastic strain increase continuously with total strain.

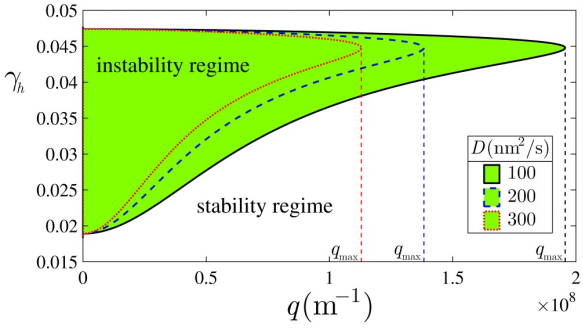

Fig. 2. Stability and instability regimes of the homogeneous deformation for various values of the free volume diffusion coefficient.

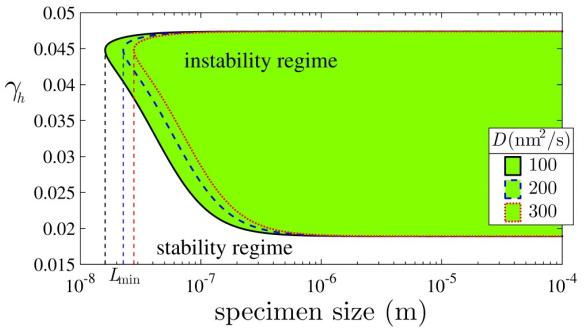

Fig. 3. Size effect on the stability-instability regimes of the homogeneous deformation for various values of the free volume diffusion coefficient.

i.e. greater values of D lead to larger stable homogeneous strains. Moreover, for layers smaller than a critical size $L_{min}:=\pi/q_{max}$ homogeneous deformations remain stable to any perturbation, i.e. the instability onset is suppressed. From a physical point of view this suggests that nanometer-scale glasses are too thin to accommodate a shear band of critical thickness. This theoretical prediction is in accordance with experimental observations reported in the literature (e.g. [34] and references quoted therein).

5. SHEAR BAND THICKNESS

As mentioned above, the stability regime and the associated size effect are strongly influenced by the free volume diffusion coefficient D and hence the length scale ℓ_ξ, while the effect of ℓ_θ and ℓ_γ on the instability initiation is rather negligible. This could give rise to a reasonable question concerning the inclusion of the strain gradient in the constitutive equation for the flow stress, which for a large variety of other materials (crystalline metals, polymers, geomaterials, etc.) has been proven to have a significant effect on the instability onset, as well as a substantial role in predicting the size of the strain localization zone (shear band or neck) and in retaining the well-posedness of boundary value problems in the softening regime. The aim of the present section is to address this question by studying the effect of the three intrinsic lengths scales on the shear band thickness, i.e. on the instability evolution rather than on its initiation.

Transmission electron microscopy (TEM) observations have demonstrated that the thickness of a shear band is in the range of 10-20 nm for a variety of metallic glasses (see, for example, the review article in Ref. [35]). This size is of the same order of magnitude with the characteristic free volume diffusion internal length $l_\xi = \sqrt{D\Delta\gamma_h / \dot{\gamma}_o}$ for the values of D and $\dot{\gamma}_o$ used in the previous section and for an increase of the homogeneous strain $\Delta\gamma_h$=0.01-0.04, i.e. within the interval shown in the graphs of Fig. 1. Accordingly, the free volume diffusion coefficient seems to control and be able to predict the aforementioned range of shear band thickness. However, recent nanoindentation tests along well-developed shear bands have revealed a zone of localized deformation and softening, which is at least three orders of magnitude larger and increases with the macroscopic plastic strain (see, for example, Refs. [36,37]). More specifically, Pan et al. [36] observed that shear band thickness grows from 40 to 160 μm as plastic strain increases from 0.02 to 0.06. As argued in that article, the reasons behind this large discrepancy could be that in TEM measurements the shear band was in its initial stage rather than fully developed, and that only the center part of the shear band is transparent enough for TEM observation. This range of thicknesses cannot be predicted by the free volume diffusion process, because it would need an increase of strain $\Delta\gamma_h$=1.6·10^5 – 2.56·10^6 to cover such a size. On the other hand, the corresponding thermal diffusion process which is determined by the characteristic heat conduction internal length $l_\theta = \sqrt{k\Delta\gamma_h / \rho c_v \dot{\gamma}_o}$ needs an increase of strain in the order of only 10^{-6} – 10^{-5}. This means equivalently that during an increase of $\Delta\gamma_h$=0.001-0.01 in strain, heat conduction covers 0.9-3 mm space. Such type of heat spreading under quasi-static loading conditions is reasonable, since temperature will be nearly uniform rather than localized because heat conduction is much faster than the deformation rate. Therefore, the observed shear

band thickness in both of the aforementioned cases and ranges cannot be associated with the thermal diffusion process.

In order to verify the above statements on the basis of our proposed model and in order to study the effect of the strain gradient coefficient on the shear band thickness, a specimen of thickness L=500 μm is considered and the system of Eqs. (3) and (4) is numerically solved with aid of the method of lines. In particular, weighted residuals (Galerkin) method is employed and the variables $\tilde{\theta}$, ξ and γ^p are interpolated in space using the spectral element method. The interior nodes of each element are distributed at the zeros of Lobatto polynomials over the canonical (local) interval [-1,1], and cubic splines with Lagrange end conditions are used for the interpolation within each element. It is noted that alternative Lagrange polynomial interpolation has been also tested giving quite similar results which are not presented here. Moreover, the same set of nodes is also used to evaluate elemental integrals according to the Gauss-Lobatto quadrature. In this connection, it is noted that other methods such as linear or C^1-continuous Hermite finite elements as well as element-free Galerkin (EFG) interpolation along with Gauss or tanh-sinh quadrature were also tested rendering rather inexact (mesh-dependent) solutions or spurious oscillations leading to propagating numerical instabilities for the same degrees of freedom. In fact, the aforementioned spectral element method is known to be superior to these schemes because of its higher order of accuracy (the computational error decreases exponentially fast as the order of approximating polynomial) and in turn, it seems to be more effective in dealing with the different orders of magnitude in the length and time scales involved in the present stiff problem.

Because of the quasi-static loading conditions, the normalized shear stress is enforced to have the same value throughout the specimen, i.e. $\tilde{\tau}=\tilde{\mu}(\gamma_{ave}-\gamma^p_{ave})$, where $\gamma_{ave}=\tilde{\dot{\gamma}}_o\,\tilde{t}$ is the average total strain and γ^p_{ave} is the average plastic strain. Moreover, periodic boundary conditions are applied for the interpolated variables, i.e.

$$\begin{aligned}
&\tilde{\theta}(\tilde{t},0)=\tilde{\theta}(\tilde{t},L),\\
&\xi(\tilde{t},0)=\xi(\tilde{t},L),\\
&\gamma^p(\tilde{t},0)=\gamma^p(\tilde{t},L),\\
&\tilde{\theta}_y(\tilde{t},0)=\tilde{\theta}_y(\tilde{t},L),\\
&\xi_y(\tilde{t},0)=\xi_y(\tilde{t},L),\\
&\gamma^p_y(\tilde{t},0)=\gamma^p_y(\tilde{t},L),
\end{aligned} \qquad (24)$$

where the subscript y denotes partial differentiation.

The initial conditions used in the previous section are also employed here, i.e. the specimen is initially strain free, has a uniform temperature field of θ_o=300K and a dimensionless free volume density ξ_o=0.05. In order to trigger the shear banding from an otherwise homogeneous field, an imperfection is assumed in the form of a 10% higher initial free volume at a narrow zone (4% of the specimen size) around the specimen center. This could be considered as a rather large imperfection, but it is chosen as such to reduce computational requirements, and it does not have any substantial influence on the band thickness under consideration, since its impact is initially reduced due to the stability of the homogeneous solution at low strains. Moreover, a non-uniform mesh is used for the discretization which becomes progressively finer at the edges of the imperfection, where the initial condition for ξ has jump discontinuities.

Since the system of ordinary differential equations resulting from the aforementioned spatial discretization is usually stiff, it is integrated with respect to normalized time by the backward differentiation formulas (Gear's method). It is also noted that in the results of the numerical calculations presented hereinafter, the distributions of plastic shear strain γ^p are normalized by γ^p_H which is its homogeneous value outside the shear band. Similarly, the free volume density measure ξ is normalized by the corresponding homogeneous value ξ_H.

In order to avoid any possible effect of discretization on the numerically predicted response, three different mesh densities consisting of N_e= 20, 40, 100 spectral elements with m= 6, 7, 10 nodes each, respectively are examined. The results are shown in Figs. 4 and 5 where the distributions of normalized plastic strain γ^p/γ^p_H and free volume density ξ/ξ_H close to the imperfection are depicted for two different values of the strain gradient coefficient, i.e. c=0 and c=5 N, and at two different loading times, i.e. when the ratio γ^p/γ^p_H takes its maximum value and when γ_{ave}=0.0475. The latter value corresponds to a state where the homogeneous solution has become stable again (see Fig. 3). It is also emphasized that the corresponding profiles of the temperature are not shown, because they are uniform and hence in accordance with the aforementioned speculation. This also suggests that the intrinsic length scale associated with heat conductivity has no effect on the shear band size for low strain rates.

It can be seen from these figures that the two finer meshes {N_e=40, m=7} and {N_e=100, m=10} give

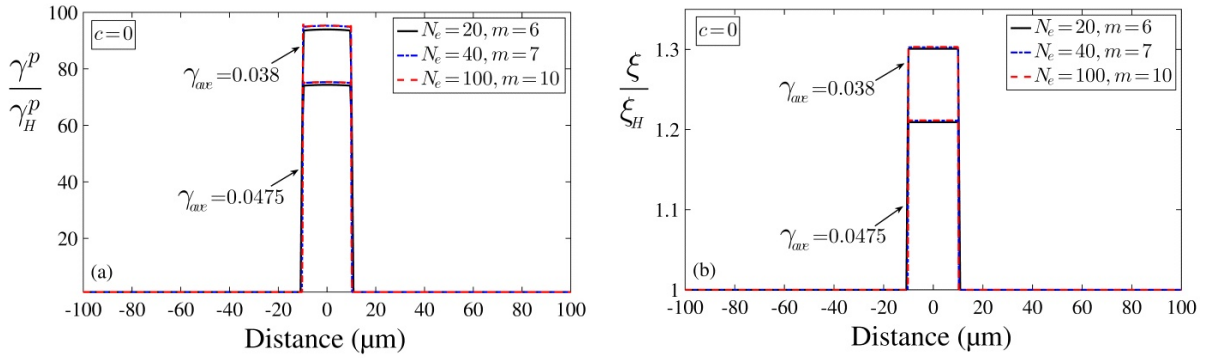

Fig. 4. Discretization sensitivity test on the profiles of the normalized plastic strain γ^p/γ_H^p and free volume density ξ/ξ_H for zero strain gradient coefficient (c=0).

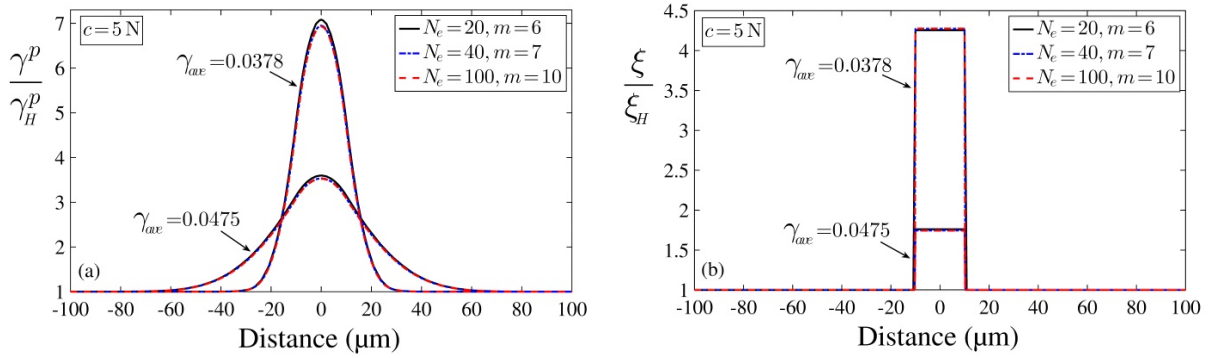

Fig. 5. Discretization sensitivity test on the profiles of the normalized plastic strain γ^p/γ_H^p and free volume density ξ/ξ_H for a nonzero strain gradient coefficient (c=5 N).

practically identical results, while the predictions of the coarser mesh is quite close to them. This suggests that taking the scheme {N_e=40, m=7} is sufficient to produce mesh-independent results.

As also shown in Figs. 4 and 5, when the strain gradient coefficient is zero, both the shear strain and free volume localization zones do not spread out of the initial imperfection region. This, in turn, implies that the intrinsic length scale associated with the free volume diffusion coefficient is not able to capture a shear band thickness in the order of micrometers, as observed experimentally [36,37]. In fact, as already discussed previously, the localization thickness in the free volume profile is exclusively determined by the diffusion internal length $l_\xi = \sqrt{D\Delta\gamma_h / \dot{\gamma}_o}$ which is up to three orders of magnitude smaller; in other words, the diffusion process is negligibly slow comparing to straining. Accordingly, the width of the imperfection remains virtually unchanged in the course of deformation. Furthermore, it is not affected by the presence of the strain gradient coefficient, which however causes an increase of the ratio ξ/ξ_H in the imperfect region due to the stress dependence entering in the reaction term of Eq. $(1)_3$.

On the other hand, the strain gradient parameter has a significant influence on the shear strain distribution by inducing a spread of the localization zone out of the initial imperfection region. This effect is investigated further by using different values of c, and the results are given in Fig. 6. It is clear from these figures that as the value of c increases, the strain profiles exhibit smoother transitions between the outside and inside regions of the band. Furthermore, the strain gradient term acts as a localization limiter in which the severity of the strain at the band reduces as c increases. Similarly, the thickness of the band increases as the value of c increases. This effect becomes more pronounced as the loading proceeds and the band diffuses further, as depicted in Fig. 7, where the values of the shear band thickness were evaluated using the width of the region surrounding the band center over which the plastic strain differs from its edge value by more than 5%.

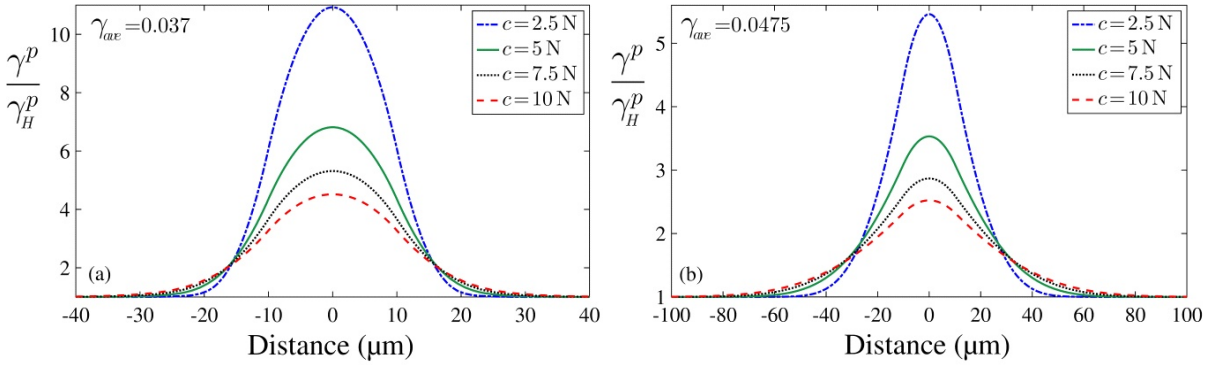

Fig. 6. Effect of the strain gradient coefficient *c* on the profiles of the normalized plastic strain.

6. CONCLUSIONS - DISCUSSION

Shear band initiation and growth have been examined in the present article by considering a coupling between gradient plasticity and thermal as well as microstructural (free volume) diffusion processes. A typical metallic glass (i.e. Vitreloy 1) has been used to estimate and illustrate the interplay between the three intrinsic material lengths (ℓ_γ, ℓ_θ, ℓ_ξ) entering the governing equations and associated respectively with the strain gradient coefficient (c), the thermal conductivity (k) and the free volume diffusion coefficient (D). It is shown that the last of these internal lengths has a dominant influence on the stability regime and the associated size effect, while the corresponding impact of the other two internal lengths is much less significant. In fact, the value of D=10^{-16} m^2/s for the free volume diffusion coefficient is very small (note that the corresponding value of the thermal diffusion process is $k/\rho c_v \cong 8.16\cdot10^{-6}$ m^2/s, and consequently it corresponds to a small characteristic ratio L_ξ^2/t_ξ, i.e. the free volume diffusion is the slowest nonlocal process involved in the model. In physical terms, this means that instability initiates when the free volume coalescence process becomes faster than diffusion leading to a microstructural softening.

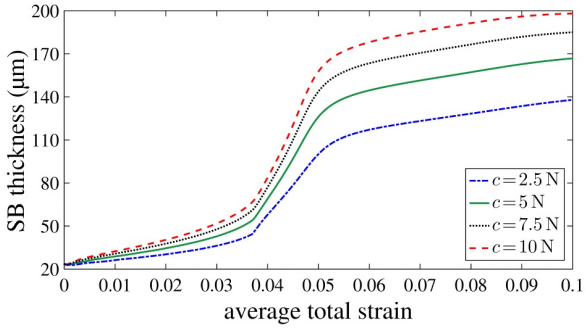

Fig. 7. Effect of the strain gradient coefficient c on the evolution of the shear band thickness.

In this connection, it is noted that this diffusion process is also able to predict shear band thicknesses in the range of 10-20 nm reported in the literature for a variety of metallic glasses [1]. However, recent studies in “cold” shear banding (i.e. shear band has essentially the uniform temperature of the bulk material) suggest a softened shear zone at least three orders of magnitude larger which thickens further as the macroscopic plastic strain increases [36]. These shear zones and their thickening cannot be described on the basis of the very slow process of the free volume diffusion or by the very fast process of thermal diffusion for the present quasi-static loading conditions. On the other hand, it is shown that the thickness of such a shear band can be predicted on the basis of strain gradients and its evolution controlled by the strain gradient length scale. In particular, the gradient term has a spreading or diffusive effect on the distribution of the plastic strain profile, as the shear band forms and grows. However, there is no corresponding influence on the free volume profile because the plastic strain variable does not enter in the reaction term $G(\xi,\theta,\tau)$ of Eq. $(1)_3$. In fact, the simplified one-dimensional shear deformation analysis presented herein enforces the rather unrealistic state of a constant shear stress τ across the specimen and, as a result, strain localization does not have a significant influence on the free volume distribution. Possible improvements of the model to account for such an effect include the consideration of its three-dimensional counterpart and/or the introduction of plastic strain gradients in $G(\xi,\theta,\tau)$. However, a more thorough study is needed in order to properly derive a

corresponding formulation, which is out of the scope of the present article, though it may serve as a suggestion for future work.

The presence of the internal length scales in the constitutive equations provides also the ability to capture size effects, i.e. the dependence of strength and other properties on the size of the specimen. In the present article, it was shown that smaller specimens can support larger homogenous deformations and the instability can be completely suppressed below a critical specimen size, which is in accordance with experimental trends [34]. It is noted that similar instability suppressions have been observed in various other processes and materials at the nanoscale as, for example, those concerning phase-separation in nanostructured intercalation systems [38], including Li-ion battery cathodes [39]. Within a continuum mechanics framework this type of size effect can be captured by utilizing the stabilizing role of higher order gradient or internal length parameters such as those emerging in gradient plasticity, in spinodal decomposition, and in diffusive-like evolution equations for internal variables (e.g. free volume).

Finally, it is pointed out that the above analysis may formally be used as a guide for capturing material instabilities in other deforming systems under micro/nanostructural changes under the influence of an externally applied or internally induced local stress, temperature, and chemical agent. The basic equations for such systems will be again the momentum (stress dynamic or static equilibrium), the energy, and an evolution equation for the dominant internal variable(s) of the reaction-diffusion type. These equations should be supplemented by constitutive assumptions, such the stress – strain relation which may be linear or nonlinear elastic, viscoelastic or viscoplastic. The multiplicity and arbitrariness in the respective choice is reduced by resorting to "subscale" discrete models and simulations, experiments, artistic intuition and ingenuity, also in concert with desired rigor and simplicity.

ACKNOWLEDGMENTS

Financial support by the General Secretariat of Research and Technology (GSRT) under the project "Internal Length Gradient Mechanics across Scales and Materials: Theory, Experiments and Applications" (ILGradMech-ASM) is acknowledged. The final version of the article was prepared with support from the Ministry of Education and Science of Russian Federation under Mega Grant Project "*Fabrication and Study of Advanced Multi-Functional Metallic Materials with Extremely High Density of Defects*" (No. 14.Z50.31.0039) to Togliatti State University.

REFERENCES

[1] A.L. Greer, Y.Q. Cheng and E. Ma // *Mat. Sci. Eng. R* **74** (2013) 71.
[2] C. Suryanarayana and A. Inoue, *Bulk Metallic Glasses - Ch. 8: Mechanical Behavior* (CRC Press, Boca Raton, 2011).
[3] C.A. Schuh and T.G. Nieh // *Acta Mater.* **51** (2003) 87.
[4] F. Spaepen // *Acta Metall.* **25** (1977) 407.
[5] P.S. Steif, F. Spaepen and J.W. Hutchinson // *Acta Metall.* **30** (1982) 447.
[6] W.L. Johnson, J. Lu and M.D. Demetriou // *Intermetallics* **10** (2002) 1039.
[7] A.S. Argon // *Acta Metall.* **27** (1979) 47.
[8] M.L. Falk and J.S. Langer // *Phys. Rev. E* **57** (1998) 7192.
[9] W.L. Johnson, M.D. Demetriou, J.S. Harmon, M.L. Lind and K. Samwer // *MRS Bull.* **32** (2007) 644.
[10] J.S. Langer // *Phys. Rev. E* **70** (2004) 041502.
[11] Y.Shi and M.L. Falk // *Phys. Rev. Lett.* **95** (2005) 095502.
[12] Q.K. Li and M. Li // *Appl. Phys. Lett.* **88** (2006) 241903.
[13] Y. Chen, M.Q. Jiang, L.H. Dai // *Int. J. Plasticity* **50** (2013) 18.
[14] M.Q. Jiang and L.H. Dai // *J. Mech. Phys. Solids* **57** (2009) 1267.
[15] E.C. Aifantis // *Mech. Res. Commun.* **5** (1978) 139.
[16] E.C. Aifantis // *Int. J. Eng. Sci.* **30** (1992) 1279.
[17] R. Huang, Z. Suo, J.H. Prevost and W.D. Nix // *J. Mech. Phys. Solids* **50** (2002) 1011.
[18] L.H. Dai, M. Yang, L.F. Liu and Y.L. Bai // *Appl. Phys. Lett.* **87** (2005) 141916.
[19] E.C. Aifantis // *J. Eng. Mater. Tech. – Trans. ASME* **106** (1984) 326.
[20] E.C. Aifantis // *Int. J. Plasticity* **3** (1987) 211.
[21] H.M. Zbib and E.C. Aifantis // *Res. Mech.* **23** (1988), 261, 279, 293.
[22] R. de Borst and H.B. Muhlhaus // *Int. J. Numer. Meth. Eng.* **35** (1992) 521.
[23] Y. Chen, L.H. Dai, Y.L. Bai and E.C. Aifantis // to appear in: *J. Mech. Behav. Mater*. (2017).
[24] Y.L. Bai // *J. Mech. Phys. Solids* **30** (1982) 195.

[25] I. Tsagrakis and E.C. Aifantis // Metall. Mater. Trans. A **46** (2015) 4459.
[26] Y.F. Gao, B. Yang and T.G. Nieh // *Acta Mater.* **55** (2007) 2319.
[27] H.M. Zbib and E.C. Aifantis // *Acta Mech.* **92** (1992) 209.
[28] R.C. Batra and Z.G. Wei // *Int. J. Impact Eng.* **32** (2006) 947.
[29] Y.L. Bai and B. Dodd, *Adiabatic Shear Localization* (Pergamon Press, Oxford, 1992).
[30] B. Dodd and Y.L. Bai, *Adiabatic Shear Localization: Frontiers and Advances* (Elsevier, London, 2012).
[31] T.W. Wright, *The Physics and Mathematics of Adiabatic Shear Bands* (Cambridge University Press, Cambridge, 2002).
[32] B. Dodd and Y. Bai // *Mater. Sci. Tech.* **5** (1989) 557.
[33] T.G. Nieh, In: *Bulk Metallic Glasses: An Overview*, ed. by M. Miller and P. Liaw (Springer, New York, 2008) p. 147.
[34] A. Donohue, F. Spaepen, R.G. Hoagland and A. Misra // *Appl. Phys. Lett.* **91** (2007) 241905.
[35] Y. Zhang and A.L. Greer // *Appl. Phys. Lett.* **89** (2006) 1907.
[36] J. Pan, Q. Chen, L. Liu and Y. Li // *Acta Mater.* **59** (2011) 5146.
[37] R. Maaß, K. Samwer, W. Arnold and C.A. Volkert // *Appl. Phys. Lett.* **105** (2014) 171902.
[38] D. Burch and M.Z. Bazant // *Nano Lett.* **9** (2009) 3795.
[39] *High Energy Density Lithium Batteries: Materials, Engineering, Applications* , ed. by K.E. Aifantis, S.A. Hackney and R.V. Kumar (Wiley-VCH, Weinheim, 2010).